AD-A170 646 SHEAR BAND CHARACTERIZATION OF MIXED MODE I AND II FULLY PLASTIC CRACK GR..(U) MASSACHUSETTS INST OF TECH CAMBRIDGE DEPT OF MECHANICAL ENGIN..

1/1

UNCLASSIFIED F A MCCLINTOCK ET AL. 31 JUL 86 F/G 11/6 NL

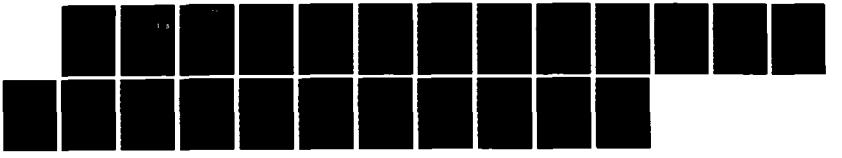

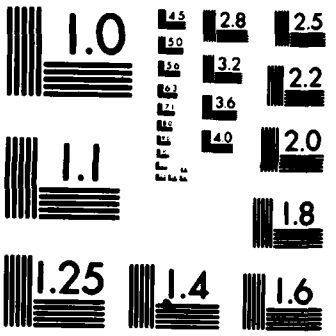

Technical Report N00014-82-k-0025 P00002 TR07

SHEAR BAND CHARACTERIZATION OF MIXED MODE I AND II FULLY PLASTIC CRACK GROWTH

Frank A. McClintock
Room 1-304, (617) 253-2219
Department of Mechanical Engineering
Massachusetts Institute of Technology
Cambridge, MA 02139

George A. Kardomateas
General Motors Research Laboratories
Engineering Mechanics Department
Warren, MI 48090-9055

Unlimited Distribution

31 July, 1986

Technical Report

Prepared for
OFFICE OF NAVAL RESEARCH
Solids Mechanics Program, Mechanics Division
Scientific Officer: Dr. Yapa Rajapakse
Code 4325 (202) 696-4306
800 N. Quincy Street
Arlington, VA 22217

SECURITY CLASSIFICATION OF THIS PAGE (When Data Entered)

REPORT DOCUMENTATION PAGE	READ INSTRUCTIONS BEFORE COMPLETING FORM
1. REPORT NUMBER: N00014-82-K-0025 P00002 TR04	2. GOVT ACCESSION NO. AD-A172646
3. RECIPIENT'S CATALOG NUMBER	
4. TITLE (and Subtitle): SHEAR BAND CHARACTERIZATION OF MIXED MODE I AND II FULLY PLASTIC CRACK GROWTH	5. TYPE OF REPORT & PERIOD COVERED: Technical Report, 31 July 1986
6. PERFORMING ORG. REPORT NUMBER	
7. AUTHOR(s): Frank A. McClintock; George A. Kardomateas (now at Eng. Mech. Dept. Gen. Motors Res. Labs., Warren MI 48090-9055	8. CONTRACT OR GRANT NUMBER(s): N00014-82-K-0025 P00002
9. PERFORMING ORGANIZATION NAME AND ADDRESS: Department of Mechanical Engineering, Massachusetts Institute of Technology, Cambridge, MA 02139	10. PROGRAM ELEMENT, PROJECT, TASK AREA & WORK UNIT NUMBERS
11. CONTROLLING OFFICE NAME AND ADDRESS: Office of Naval Research, Solid Mechanics Program, Mech. Div. Code 432S, 800 N. Quincy St., Arlington, VA 22217	12. REPORT DATE: 31 July 1986 13. NUMBER OF PAGES: 18
14. MONITORING AGENCY NAME & ADDRESS(if different from Controlling Office)	15. SECURITY CLASS. (of this report): Unclassified 15a. DECLASSIFICATION/DOWNGRADING SCHEDULE

16. DISTRIBUTION STATEMENT (of this Report)
Distribution unlimited

17. DISTRIBUTION STATEMENT (of the abstract entered in Block 20, if different from Report)

18. SUPPLEMENTARY NOTES

19. KEY WORDS (Continue on reverse side if necessary and identify by block number)
Ductile fracture, shear band, theory, experiments, crack opening angle, fracture stable design

20. ABSTRACT (Continue on reverse side if necessary and identify by block number)
Fully plastic crack growth in singly grooved tensile specimens is characterized locally by the directions and amounts of fracture and slip on various planes. The model relates macroscopic quantities, including the crack growth ductility, defined as the axial displacement per unit ligament reduction, which is of practical importance in determining the stiffness of the surrounding structure that is needed to prevent unstable fracture. (cont.)

DD FORM 1 JAN 73 1473 EDITION OF 1 NOV 65 IS OBSOLETE
S N 0102-LF-014-6601

SECURITY CLASSIFICATION OF THIS PAGE (When Data Entered)

Applied to six different structural alloys with strain-hardening exponents from 0.1 to 0.2, the model gave crack-growth ductilities within 10% for the symmetrical configurations, where the value ranged from 0.25 to 0.4, and were unrelated to the strain-hardening exponent.

For the asymmetrical configurations that occur near welds or shoulders, the crack growth ductility for the low hardening materials drops to 0.07 to 0.11. The predicted values were uniformly high by a factor of two, providing a good relative ranking of the alloys.

Other macroscopic correlations were generally within 10%. Thus this slip plane model of fully plastic crack growth provides a useful correlation between macroscopic measurements made on the specimens after fracture, and the important loss of crack growth ductility that occurs in asymmetric configurations with materials with low strain-hardening.

Shear Band Characterization of Mixed Mode I and II Fully Plastic Crack Growth

by F.A. McClintock and G.A. Kardomateas

Abstract

Fully plastic crack growth in singly-grooved tensile specimens is characterized locally by the directions and amounts of fracture and slip on various planes. The model relates macroscopic quantities, including the crack growth ductility, defined as the axial displacement per unit ligament reduction, which is of practical importance in determining the stiffness of the surrounding structure that is needed to prevent unstable fracture.

Applied to six different structural alloys with strain-hardening exponents from 0.1 to 0.2, the model gave crack growth ductilities within 10% for the symmetrical configurations, where the values ranged from 0.25 to 0.4 and were unrelated to the strain-hardening exponent.

For the asymmetrical configurations that occur near welds or shoulders, the crack growth ductility for the low hardening materials drops to 0.07 to 0.11. The predicted values were uniformly high by a factor of two, providing a good relative ranking of the alloys.

Other macroscopic correlations were generally within 10%. Thus this slip plane model of fully plastic crack growth provides a useful correlation between macroscopic measurements made on the specimens after fracture, and the important loss of crack growth ductility that occurs in asymmetric configurations with materials with low strain-hardening.

Introduction

If a structure cracks, it is desirable that any crack growth be fully plastic to provide large deflections, both for stability by load-shedding to other parts of the structure, and for facilitating crack detection before failure of the entire structure. This desired crack growth

ductility is reduced by asymmetry, which tends to focus the deformation into a single band, along which the crack advances into pre-damaged material. With symmetry, on the other hand, the crack tends to advance between two slip bands into undamaged material. Kardomateas and McClintock [1] have found that for plane strain tension applied to singly-grooved specimens of low strain-hardening alloys (strain-hardening exponent $n \approx 0.1$), asymmetric, (mixed Mode I and II) specimens showed only 1/3 the crack growth ductility of symmetric (Mode I) ones. (This reduction is much less pronounced for crack initiation and for $n \approx 0.2$.) The object here is to characterize the local sliding-off and fracture processes in terms of macroscopic observations of deformation.

Strain-hardening materials require a finite element analysis, perhaps coupled with a rigid-plastic singularity [2], and in turn at the very tip, if not dominated by the fracture process zone itself, an elastic-plastic singularity (Ponte-Castañeda [3]). Even when these analyses can be successfully combined, there will be a need for an approximate characterization in simple terms. Here we consider such an analysis based on at most one band above, and one below, a growing crack. In singly-grooved specimens of non-strainhardening material, such bands would be at $\pm$ 45°. In doubly-grooved specimens under tension, or for linearly strainhardening materials, the deformation may occur in a fan, which would be approximated by a slip band at more than 45° from the axis.

For slightly asymmetric specimens, with bands above and below the normal to the tensile axis, Kardomateas [4] found the relative amounts and the angles of sliding on the two slip planes, and of fracture on an intermediate plane, in terms of the angles and projected lengths of the fracture surfaces and one of the angles of deformation of the back surface. While this analysis also gives the symmetric case, it requires that slip on the two planes be of opposite sign, and thus does not apply to the strongly asymmetric configurations of interest here.

Analysis for Asymmetric Configurations

With sufficient asymmetry, both slip lines lie above the axis

transverse to tension. Then the shear on both will be of the same sign. As shown in Figs. 1a,b, the crack growth direction may lie below both lines or below just one. (If it were to lie above both, crack closure would prevent any deformation; the limit of a crack growth direction parallel to the upper band would be pure Mode II.) In the field of Fig. 1a, the deformation on the back surface is entirely above the point at which the crack breaks through to the back surface; the field of Fig. 1b has deformation both above and below. (Remember the goal here is an approximate characterization: the fields are both unrealistic for non-hardening plasticity in that the slip directions would both have to be 45°, and in Fig. 1b the lower slip line would split into a fan rather than break through to a convex point on the back surface.)

Next turn to the local process, shown in Fig. 2. The amounts of sliding on the two slip lines and of fracture are denoted by s_u, s_ℓ, and f, and the respective directions by θ_u, θ_ℓ, and θ_f. The ratios of s_u, s_ℓ, and f are assumed constant during crack growth, so in what follows s_u, s_ℓ, and f can also represent the total contribution of each to crack growth across the entire ligament ℓ_0. Consider a cycle of first sliding on the upper plane, then on the lower, and finally fracture. In Fig. 2, both slip lines lie above the fracture direction, and the new surface generated by sliding off lies entirely on the lower surfaces. The upper flank of the crack consists solely of fracture surface. Furthermore, the length and angle of lower flank depend only on the resultant of slip on the two slip lines, not on their partitioning. The only way of distinguishing between the two components of slip would be through the shape of the deformed back surface, as shown in Fig. 1. This shape is so dependent on strain-hardening that the analysis will not be carried out here. Instead, the two slip lines will be combined into one, with slip s in the direction θ_s.

First consider the equations for the flanks. From Fig. 2 the upper surface is produced entirely by the fracture:

$$\theta_u = \theta_f \quad . \tag{1}$$

For the lower flank angle, (Fig. 2)

$$\tan\theta_{\ell} = \frac{f \sin\theta_f + s_{\ell}\sin\theta_s}{f \cos\theta_f + s_{\ell}\cos\theta_s} \quad . \tag{2}$$

Because the fracture angle is below both of the slip angles, there is no deformation below the lower flank angle, and the projection of the lower flank length is just the original value:

$$\ell_{\ell} = \ell_0 = f \cos\theta_f + s \cos\theta_s \quad . \tag{3}$$

Because the upper flank consists solely of fracture surface, the projected upper ligament length is:

$$\ell_u = f \cos\theta_f \quad . \tag{4}$$

In principle, Eqs. 2-4 allow determining the microscopic quantities f , s , and θ_s from the macroscopic variables θ_{ℓ} , ℓ_{ℓ} , and ℓ_u . In practice, the crack opening angle $\theta_{\ell} - \theta_u$ is too small for good accuracy. It turns out to be more accurate to base the microscopic variables on the back angle of Fig. 3 (see also Fig. 1), which is the deformed region resulting from the slip line sweeping past points on the back surface:

$$\tan\beta = \frac{s \cos\theta_s}{s \sin\theta_s + f(\sin(\theta_s - \theta_f))/\cos\theta_s} \quad . \tag{5}$$

The microscopic parameters can now be found from Eqs. 2-4 as follows. With θ_f equal to the upper flank angle according to Eq. 1, the fracture extent f can be found from Eq. 4. Solving Eq. 3 for s , introducing it into Eq. 4 and expanding the denominator gives

$$\tan\beta = \frac{\ell_0 - f \cos\theta_f}{(\ell_0 - f \cos\theta_f)\tan\theta_s + f \tan\theta_s \cos\theta_f - f \sin\theta_f} \quad , \tag{6}$$

which can be solved explicitly for $\tan\theta_s$ in terms of known quantities:

$$\tan\theta_s = f \sin\theta_f + \frac{\ell_0 - f\cos\theta_f}{\tan\beta} \quad . \tag{7}$$

With θ_s known, the slip ratio s can now be found from Eq. 3 with θ_f from Eq. 1 and f from Eq. 4.

From these microscopic parameters, a number of other variables can be found for comparison with data:

The lower flank angle θ_ℓ is found from Eq. 2.

The projected lower flank ratio ℓ_ℓ should be ℓ_0, since from Fig. 2 there is no deformation below the lower flank.

The crack growth ductility, defined as the total axial displacement per unit ligament reduction, is

$$D_g = \frac{u_y}{\ell_0} = \frac{s}{\ell_0}\sin\theta_s \quad . \tag{8}$$

An apparent crack ductility for the lower flank can be defined as the *projection of the shear-exposed surface* onto the total flank surface. It has been roughly estimated fractographically as the ratio of hole growth to sliding-off area (Kardomateas, 1986). Since the ratio of shear displacement to original ligament width is s, and the material below the lower flank is undeforming.

$$D_{AC\ell} = \frac{s\cos(\theta_s - \theta_\ell)}{\ell_0\cos\theta_\ell} \quad . \tag{9}$$

Since the upper flank in this model is generated entirely by fracture,

$$D_{ACu} = 0 \quad . \tag{10}$$

Some measure of how sorely tried the non-hardening assumption is can be found from the thickness of the slip band, again in units of original ligament thickness, and the strain in the band, both found from Fig. 3:

$$t_{sb} = f \sin(\theta_s - \theta_f) \quad . \tag{11}$$

$$\gamma = s/t_{sb} \quad . \tag{12}$$

Now suppose the lower slip line lay below the fracture direction, but above the transverse direction. In contrast to the case of Fig. 2 analyzed above, slip on the lower line would turn out to increase lower projected ligament length above its original value. Since this was not observed, it will not be analyzed here.

Analysis for Symmetrical Configurations

The model for symmetrical crack growth is shown in Fig. 4. The macroscopically observable variables are the crack flank angle (or the opening half-angle) $\theta_c \equiv COA/2$, and the projected crack flank length at separation ℓ , which turns out to be shorter than the original ligament length ℓ_0 . The corresponding microscopic variables are the amounts of fracture f and sliding s , and the angle of the slip line relative to the transverse direction, θ_s . The three microscopic variables are found from
first the projected crack flank length,

$$\ell = s\cos\theta_s + f \; ; \tag{13}$$

the crack flank angle,

$$\tan\theta_c = \frac{s\sin\theta_s}{f + s\cos\theta_s} \; ; \tag{14}$$

and the original ligament dimension, which is ℓ plus the sliding-off that deforms the back side:

$$\ell_0 = f + 2s\cos\theta_s \quad . \tag{15}$$

Equations 13-15 can be solved by eliminating f from Eqs. 14 and 15

with Eq. 13, and solving each for s :

$$s = \frac{\ell \tan\theta_c}{\sin\theta_s} = \frac{\ell_o - \ell}{\cos\theta_s} \quad ; \tag{16}$$

$$\tan\theta_s = \tan\theta_c \frac{\ell}{\ell_o - \ell} \quad . \tag{17}$$

With θ_s known, s is found from either of Eqs. 16 and f from Eq. 13.

The back angle is found from the construction of Fig. 4:

$$\tan\beta = \frac{s \cos\theta_s}{f \tan\theta_s + s \sin\theta_s} \quad . \tag{18}$$

The crack growth ductility D_g can be conviently expressed in terms of either the microscopic or macroscopic variables.

$$D_g = \frac{u_y}{\ell_o} = \frac{2s \sin\theta_c}{\ell_o} = \frac{2\ell \tan\theta_c}{\ell_o} \quad . \tag{19}$$

The apparent crack ductility (the projection of the shear-exposed surface onto the total flank surface) is

$$D_{AC} = \frac{s \cos(\theta_s - \theta_c)}{s \cos(\theta_s - \theta_c) + f \cos\theta_c} \quad . \tag{20}$$

The thickness of the slip band and the strain in it are found from Eqs. 11 and 12, with $\theta_f = 0$.

Comparison with Experimental Results

Tensile tests on symmetrical and asymmetrical singly-grooved, fully plastic specimens were carried out on the six structural alloys summarized in Table 1 [1]. The 1018 cold-finished and the HY-80 and HY-100 steels showed low strain hardening ($n \approx 0.1$), the normalized 1018 and the hot-rolled 1018 steel showed higher hardening ($n \approx 0.2$), and the 5086-H111 aluminum was intermediate.

For symmetrical specimens, the results of the shear-band

characterization are shown in Table 2. The different levels of strain-hardening had little effect.

a) There was some tendency for the higher hardening alloys to have slip angles θ_s farther below the non-hardening value of 45°, as observed previously (e.g. for annealed commercially pure aluminum [5]).

b) The crack growth ductilities deduced from Eq. 18 all fell in the range of 0.24 to 0.39 and were within 0.03 of the observed values.

c) While most of the deduced back angles β were within 2° of the observed values, for two of the higher-hardening alloys the deduced back angle was high by a factor of up to 1.5, perhaps due to spreading out of the slip band with more hardening.

d) The deduced apparent crack ductilities D_{AC} were all between 0.24 and 0.38, a factor of two below the observed values [6]. This indicates that the local process was by no means as well characterized as the macroscopic one.

For asymmetrical specimens, the results of the shear-band characterization are shown in Table 3. Here the various parameters are predicted from the relative projected ligament length ℓ_u/ℓ_0 and angle θ_u of the upper flank, and the back angle β. The different levels of strain-hardening had a substantial effect.

a) The deduced slip angle θ_s increases with strain hardening, although not quite as rapidly as observed from relative end-to-end motion. It is larger than 45°, indicating a Mode I component of displacement which is not adequately modelled by the single shear band, especially for higher hardening. The slip angle is greater than the cracking angle $\theta_f = \theta_u$, as assumed for these equations.

b) The lower flank angle θ_ℓ is no more than 2° above that observed, but this difference is a relatively large fraction of the crack opening angle, $\theta_\ell - \theta_u$ = 1 to 6° .

c) The projected lower flank ratio ℓ_ℓ/ℓ_0 should be unity if the slip were concentrated on a single plane above the cracking direction. The observed values of 0.90 to 0.87 are generally lower for higher hardening, and are an indication that the single slip-band model is less exact for higher hardening and near-tip phenomena.

d) The deduced crack growth ductility D_g is about double that observed, and both decrease by a factor of 2-3 for lower strain-hardening.

e) The deduced apparent crack ductility , as with symmetrical specimens, is much less than observed. The correct trends are present, however, with more apparent crack ductility on the lower surface than the upper, and more with higher hardening than with lower hardening.

f) The single slip model discussed above fails to include the opening mode, which could be introduced by considering slip on a plane below the transverse axis. This would have the further advantage that some slip, or apparent crack ductility, would appear on the upper flank. Such an analysis [4], when applied to the data, gave both slip angles above the transverse axis, in contradiction with the assumption. Thus the single-slip model discussed here seems to be the best that can be done with one or two slip-planes, at whatever angles.

Conclusions

Fully plastic crack growth in singly-grooved tensile specimens was modelled by a combination of fracture on one plane and slip on another pair, for symmetric configurations, or slip on another single plane, for asymmetric configurations. Macroscopic measurements allow characterizing the crack growth locally by the directions and amounts of fracture and slip. The macroscopic measurements also give other macroscopic quantities, such as the angle of the deformed surface on the back side of the specimen and the crack growth ductility, defined as the axial displacement per unit ligament reduction (as observed by the fractional drop in the load during crack growth). The crack growth ductility is of practical importance in determining the stiffness of the surrounding structure that is needed to prevent unstable fracture.

Applied to six different structural alloys with strain-hardening exponents from 0.1 to 0.2, the model gave crack growth ductilities within 10% for the symmetrical configurations, where the values ranged from 0.25 to 0.4 and were unrelated to the strain-hardening exponent. Correlations with back angle were within 25%, with one exception.

For the asymmetrical configurations that occur near welds or shoulders, the crack growth ductility for the low hardening materials drops to 0.07 to 0.11 for the low-hardening alloys. The predicted values were uniformly high by a factor of two. The slip-band model thus provided a good relative ranking of materials in regard to this important loss of ductility. Correlations with the end-to-end displacement direction and with the lower projected ligament length and flank angle were all within 10%.

This slip plane model of fully plastic crack growth therefore provides a useful correlation between macroscopic measurements made on the specimens after fracture, and the important loss of crack growth ductility that occurs in asymmetric configurations with materials with low strain-hardening.

Acknowledgements

The analysis for the asymmetric case was carried out in part by Mary E. David. The financial support of the Office of Naval Research, Arlington, Virginia, Contract N00014-82K-0025, and the interest of the Project Monitor, Dr. Y. Rajapakse, are gratefully acknowledged. M.T. Manning cheerfully provided valuable editorial assistance.

References

1. Kardomateas, G.A. and McClintock, F.A., "Tests and Interpretation of Mixed Mode I and II Fully Plastic Fracture from Simulated Weld Defects", ONR Technical Report N00014-82-K-0025 TR06 (1986).
2. Kardomateas, G.A., "On the Fully Plastic Flow past a Growing Asymmetric Crack and its Relation to Machining Mechanics", Chap. 6 in 'Mixed Mode I and II Fully Plastic Crack Growth from Simulated Weld Defects', PhD Thesis, M.I.T. Department of Mechanical Engineering (1985).
3. Ponte-Castañeda, P. "Asymptotic Fields in Steady Crack Growth with Linear Strain-Hardening", submitted to J. Mech. Phys. Solids, (1985).
4. Kardomateas, G.A. "Shear-Band Characterization of Mixed Mode I and II

Fully Plastic Crack Growth", Chap. 4 in Thesis of [2], (1985).

5. McClintock, F.A., and Argon, A.S., eds. 'Mechanical Behavior of Materials' Addison Wesley, Reading MA, p. 378 (1966).

6. Kardomateas, G.A., "Fractographic Observations in Asymmetric and Symmetric Fully Plastic Crack Growth", Scripta Met. 20, 609-614 (1986).

Table 1. Room temperature tensile and hardness data for the six alloys tested.

Yield strength, strain	Tensile strength, unif.strn	Hard-ness	RA	Fracture true strg, strn		Parameters: $\sigma = \sigma_1(\epsilon+\epsilon_0)^n$ strength	pre-strain	expo-nent
YS, ϵ_y	TS, ϵ_u	"HDP"		σ_f	ϵ_f	σ_1	ϵ_0	n
MPa, -	MPa, -	kgf/mm^2	%			MPa	-	-
1018 steel, (0.15-0.20% C, 0.60-0.90% Mn) cold finished								
580 0.002	614 0.02	163	75	760	0.70	800	0.072	0.12
(The above are typical values; tests being re-run)								
HY-80 steel, (0.18% C, 2-3.25% Ni, 0.10-0.40% Mn, 0.15-0.35% Si)								
648 0.002	745 0.13	209	71	1200	1.25	1030-1150	0.007-0.043	0.10-0.17
HY-100 steel, (0.20% C, 2.25-3.50% Ni, 0.10-0.40% Mn, 0.15-0.35% Si)								
772 0.002	869 0.072	248	71	1350	1.24	1100-1280	0.001-0.111	0.06-0.18
5086-H111 aluminum, (4% Mg, 0.4% Mn, 0.15% Cr)								
225 0.002	333 0.15	82	44	480	0.58	510-540	0.002-0.010	0.15-0.18
1018 steel, normalized 1700°F in argon								
351 UYP								
305 0.028	457 0.17	103	70	830	1.19	690-770	-0.025-0.100	0.14-0.27
A36 steel. (0.29% max C. 0.60-0.90% Mn) hot rolled								
411 UYP								
327 0.032	469 0.24	90	68	880	1.14	800-840	-0.020-0.022	0.20-0.26

Table 2 Characterization of Singly-grooved Symmetrical Fracture

Alloy	1018 CF	HY-80	HY-100	5086-H111	1018 Norm	A36 HR
Observations						
Projected flank ratio, ℓ/ℓ_0	0.74	0.80	0.78	0.75	0.74	0.78
Crack flank angle, θ_c	9^0	13^0	14^0	9^0	12^0	10^0
Corresponding Local Parameters						
Slip angle, θ_s	36^0	43^0	41^0	25^0	31^0	32^0
Slip ratio, s/ℓ_0	0.22	0.27	0.29	0.28	0.30	0.26
Fracture ratio, f/ℓ_0	0.64	0.60	0.56	0.50	0.48	0.56
Dependent Variables						
Crack growth ductility, $D_g = u_y/\ell_0$						
deduced	0.26	0.37	0.39	0.24	0.31	0.28
observed	0.26	0.36	0.40	0.23	0.32	0.25
Back angle, β_u						
deduced	12^0	10^0	12^0	23^0	19^0	16^0
observed	12^0	12^0	13^0	16^0	15^0	15^0
Apparent crack ductility, D_{AC}						
deduced	0.24	0.29	0.32	0.35	0.38	0.30
observed	0.67					0.68
Shear band thickness, t_s/ℓ_0	0.59	0.68	0.66	0.43	0.52	0.53
Shear band strain, γ	0.38	0.40	0.44	0.64	0.59	0.49

Table 3 Characterization of Singly-grooved Asymmetrical Fracture Based on back angle β instead of lower flank angle θ_ℓ

Alloy	1018 CF	HY-80	HY-100	5086-H111	1018 Norm	A36 HR
Observations						
Projected upper flank ratio, ℓ_u/ℓ_0	0.89	0.85	0.82	0.81	0.75	0.77
Upper flank angle, $\theta_u = \theta_f$	40^0	39^0	39^0	39^0	36^0	36^0
Back angle, β_u	13^0	12^0	14^0	15^0	13^0	13^0
Corresponding Slip and Fracture Parameters						
Slip angle, θ_s						
deduced	51^0	54^0	54^0	54^0	56^0	57^0
observed	51^0	55^0	55^0	56^0	63^0	61^0
Slip displacement ratio, s/ℓ_0	0.17	0.26	0.31	0.32	0.48	0.42
Fracture length ratio, f/ℓ_0	1.16	1.09	1.06	1.04	0.93	0.95
Dependent Variables						
Lower flank angle, θ_ℓ						
deduced	41^0	42^0	42^0	42^0	44^0	43^0
measured	41^0	41^0	41^0	41^0	42^0	41^0
Projected lower flank ratio, ℓ_ℓ/ℓ_0						
deduced	1.0	1.0	1.0	1.0	1.0	1.0
observed	0.96	0.93	0.90	0.89	0.87	0.89
Crack growth ductility, $D_g = u_y/\ell_0$						
deduced	0.14	0.21	0.25	0.26	0.41	0.36
load-ext	0.07	0.10	0.10	0.11	0.22	0.18
Apparent crack ductility on upper flank, D_{ACu}						
deduced	0	0	0	0	0	0
SEM meas	0.37					0.57
Apparent crack ductility on lower flank, $D_{AC\ell}$						
deduced	0.13	0.19	0.22	0.23	0.33	0.30
SEM meas	0.52					0.68
Shear band thickness ratio, t_s/ℓ_0	0.22	0.29	0.28	0.27	0.35	0.34
Shear band strain, γ	0.80	0.89	1.11	1.21	1.35	1.23

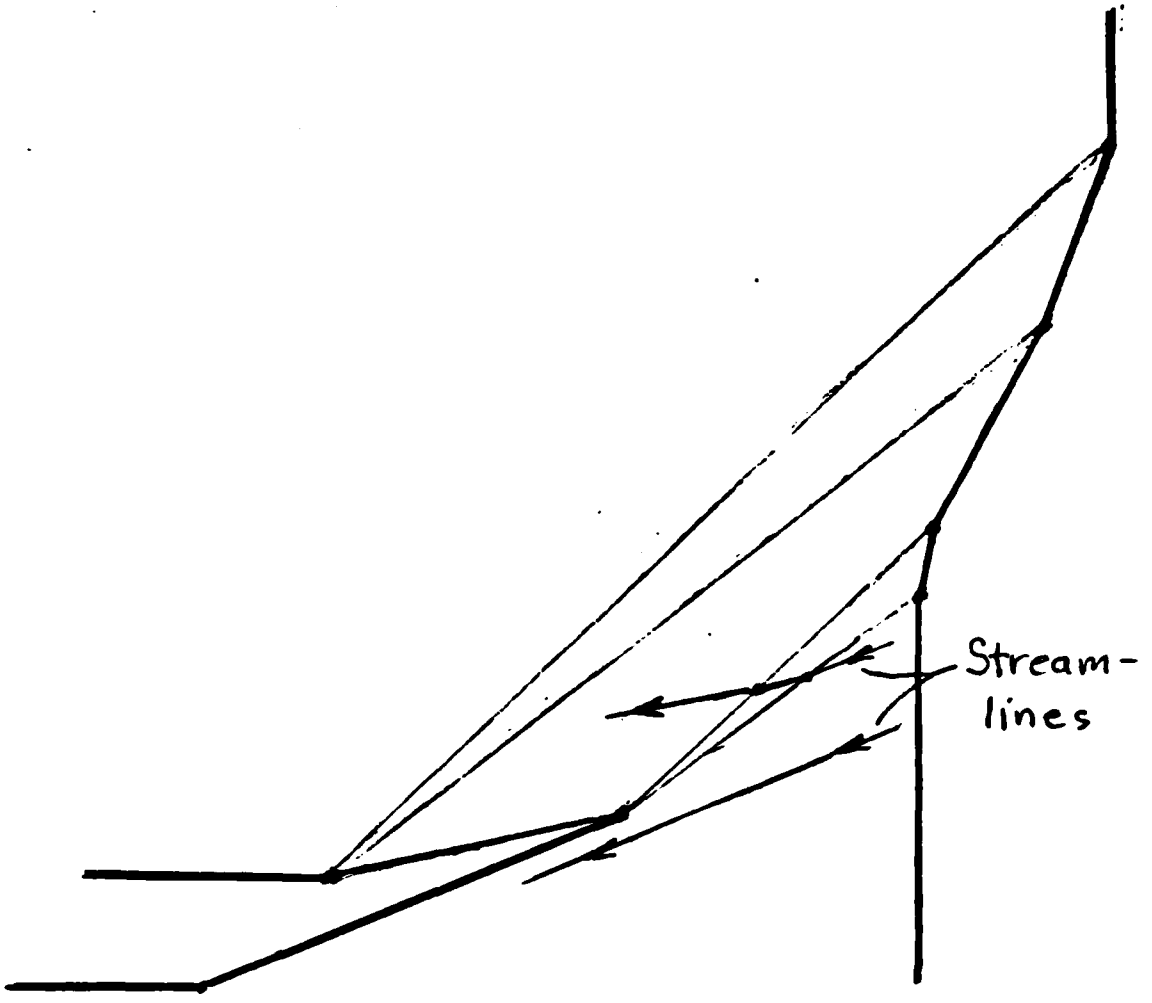

Fig. 1a Streamlines for crack advancing below two slip lines with same sign of shear.

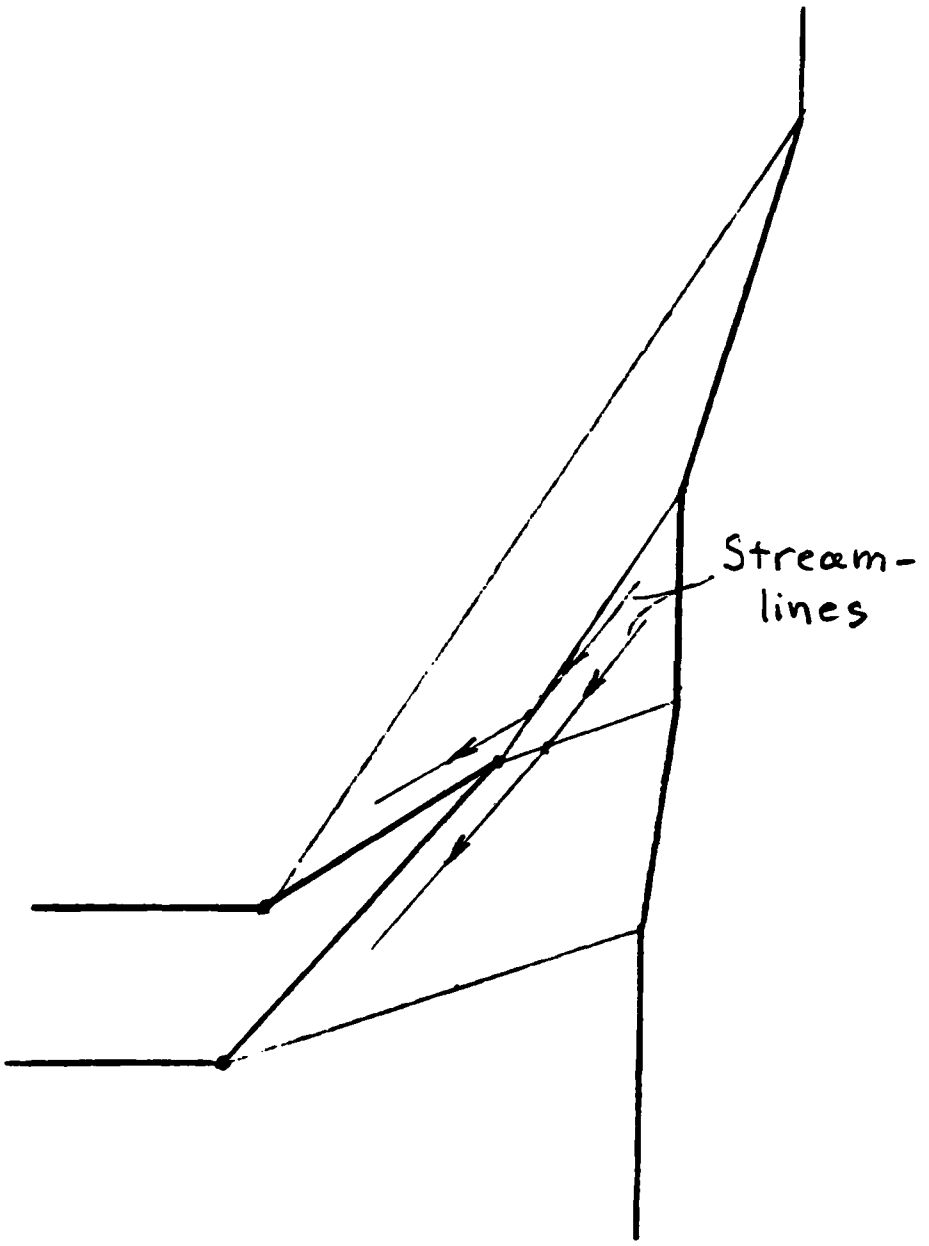

Fig. 1b Streamlines for crack advancing between two slip lines with same sign of shear

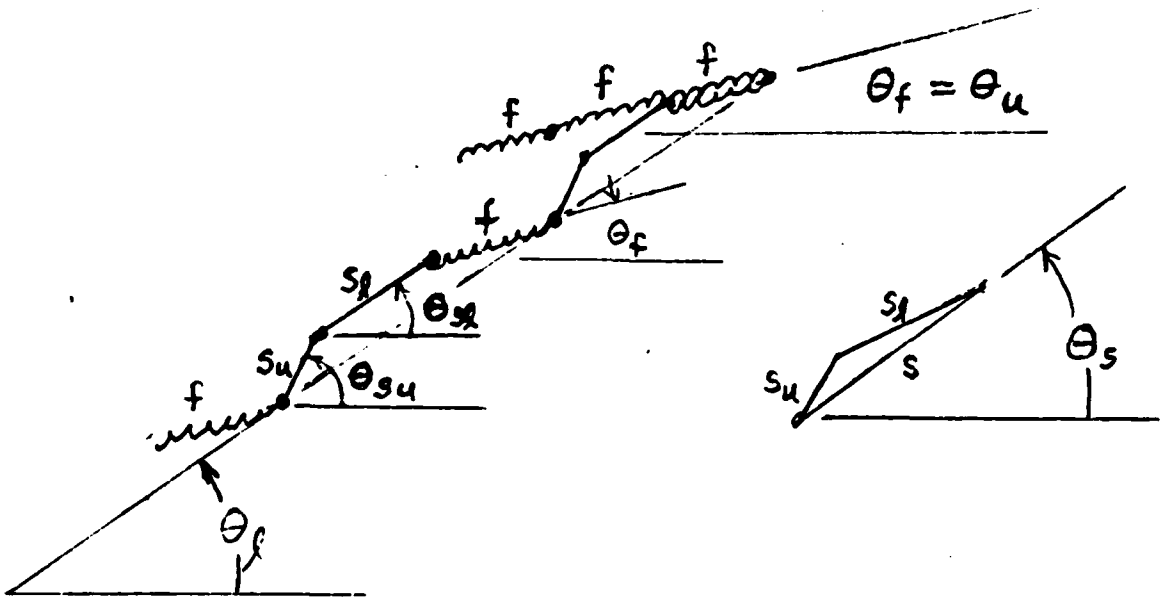

Fig. 2 Details of crack growth by alternating slip and fracture, with fracture below both slip planes. Note equivalence of two-band and single-band models.

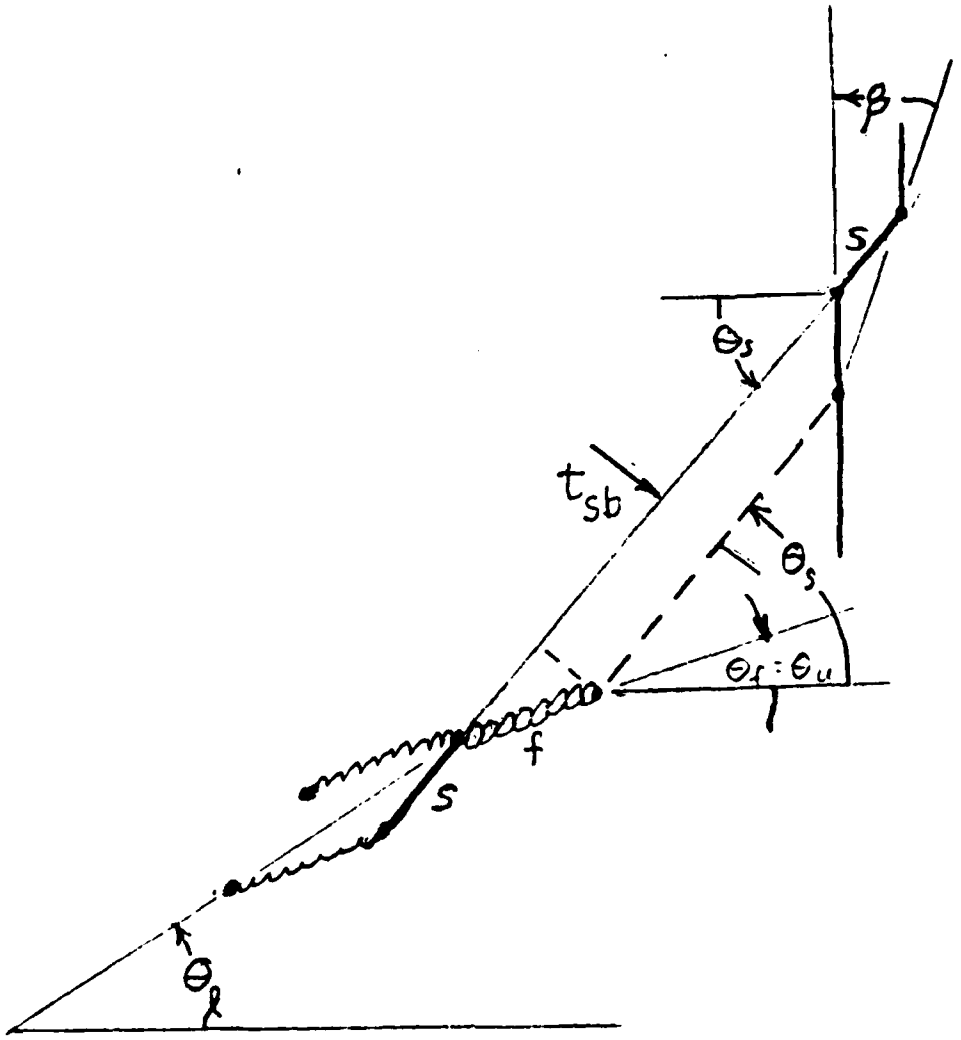

Fig. 3 Construction for finding back-angle, and shear-band strain.

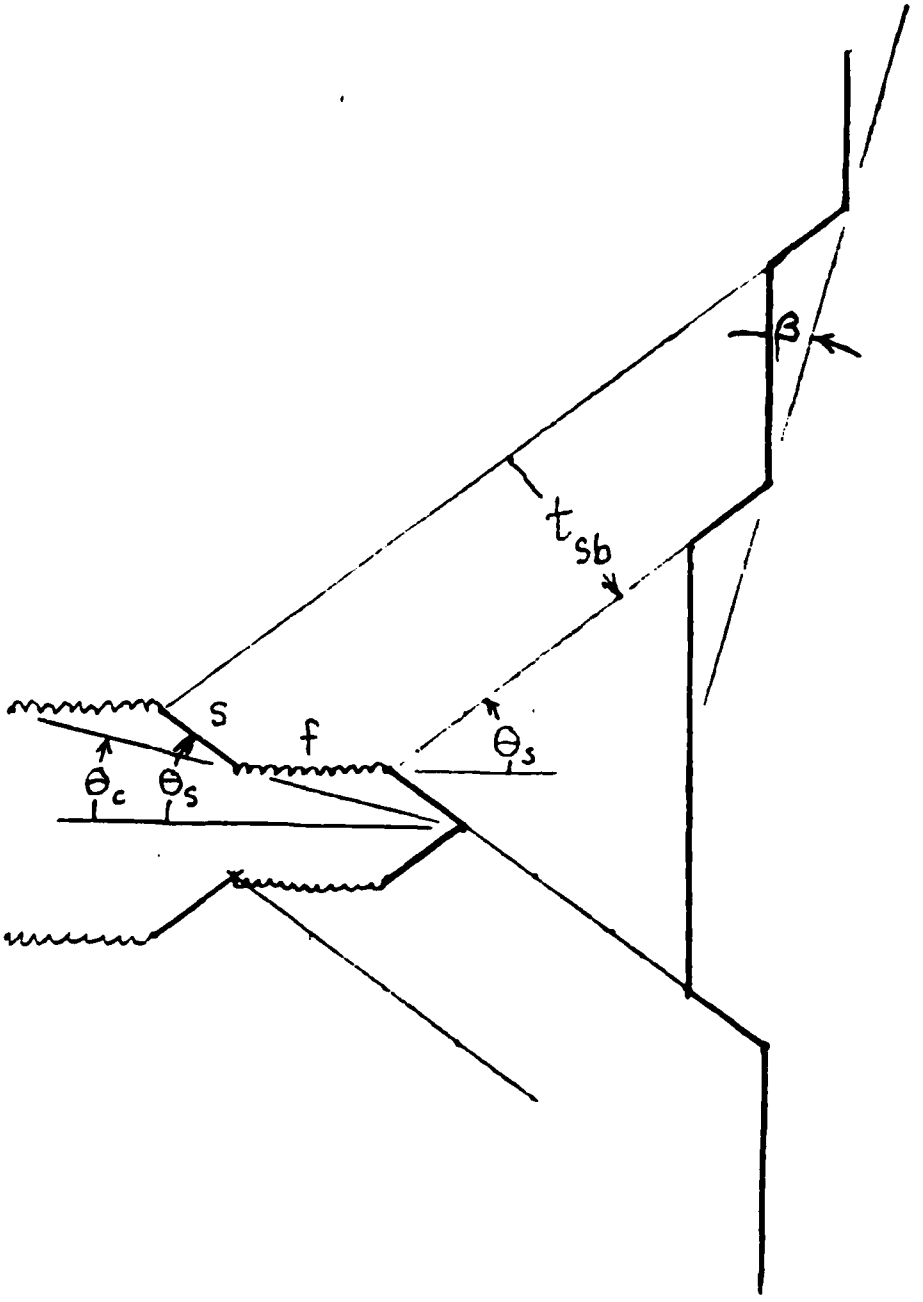

Fig. 4 Construction for symmetrical crack.

END

DTIC

9-86